

Investigation of the eddy current effect on the high frequency response of the Mirnov probe on J-TEXT

Chengshuo Shen¹, Zhenming Cai¹, Tian Ren¹, Xitong Zhang¹, Qiming Hu², Nengchao Wang^{1, a}, Zhuo Huang¹, Song Zhou¹, Jianchao Li³, Mao Li¹, Da Li¹, Dongliang Han¹ and Yonghua Ding¹

¹International Joint Research Laboratory of Magnetic Confinement Fusion and Plasma Physics, State Key Laboratory of Advanced Electromagnetic Engineering and Technology, School of Electrical and Electronic Engineering, Huazhong University of Science and Technology, Wuhan, 430074, People's Republic of China

²Princeton Plasma Physics Laboratory, PO Box 451, Princeton, NJ 08543, United States of America

³Advanced Energy Research Center, Shenzhen University, Shenzhen 518060, People's Republic of China

Abstract: This paper investigates the high frequency response of the Mirnov probe based on a test platform, which is capable of generating a uniform AC magnetic field within the frequency range of 1-300 kHz. The eddy current effect is quantitatively reflected by the phase shift ϕ_c and normalized amplitude δ of the measured magnetic field between cases with and without a conducting plate located near the Mirnov probe. This method compensates the resonant effect in the Mirnov probe circuit, and hence reflects purely the eddy current effect. The eddy current effect increases with the decrease of the distance between the probe and the conducting plate. With the increase of frequency, the magnitude of δ decreases to a saturated value at 10 kHz but increases significantly above 100 kHz for 304-stainless steel, while the eddy current effect with graphite appears at around 10 kHz and the magnitude of δ decreases to the minimum at 125 kHz, followed by a significantly increase above 125 kHz. With the increase of f , the magnitude of ϕ_c increased until 2.5 kHz and 40 kHz for steel and graphite respectively, then decreased with further increase of f . The phasor expression is introduced to describe the AC magnetic field and allows an easy expression of the eddy current field. The phase of the eddy current field decreases towards -180° with f . The amplitude of the eddy current field increase with f and reaches its maximum when the skin depth reduces to a critical value. The eddy current field decreases with further increase of the frequency.

I. INTRODUCTION

Magnetohydrodynamic (MHD) instability is an important topic in magnetic confined fusion research, such as in tokamaks [1]. The appearance of MHD instabilities is usually accompanied by high frequency perturbations of the magnetic field. Magnetic inductive coils, also named as Mirnov probes, have been widely applied to measure these perturbations of the magnetic field in tokamaks and stellarators since 1970s [2, 3]. The frequency of MHD instabilities ranges mainly from a few kilohertz to beyond a few hundred kHz [4], hence the high frequency response of the Mirnov probe is of great importance in measuring these instabilities.

Extensive studies have been carried out to investigate, understand and calibrate the high frequency magnetic measurements on several tokamaks. There are two key issues, which influence the high frequency measurement: the frequency response of the electronics and the eddy current effect. The first issue can be addressed through calibration by determining the lumped-circuit parameters of the magnetic probe and corresponding electronics, as shown in J-TEXT [5]. Additionally, a new remote calibration technique, which accounts for the presence of the first few LRC circuit resonances, has also been used to calibrate in the range 30–460 kHz on JET. [6] The high frequency magnetic perturbations, generated

by MHD instabilities, induce eddy currents in the conductors near the probes. As a result, magnetic perturbations measured by the probes might exhibit significant phase shift and normalized amplitude with respect to that from MHD instabilities. The eddy currents in the vessel wall and in-vessel components were modelled by the time varying perturbation fields on ASDEX Upgrade [7], the Mirnov measurements were better interpreted and the previously unseen MHD modes were revealed. The high frequency response of the Mirnov probes was also measured in-situ [8] and the corresponding transfer functions were successfully applied to reduce the systematic errors in identifying the toroidal mode numbers for the frequency range from 50 to 250 kHz on ASDEX Upgrade [9].

Several high frequency MHD instabilities have been observed on J-TEXT, such as the rotating tearing modes at a few kHz [10], sawtooth precursor modes and the Beta-induced Alfvén Eigenmode (BAE) from 20 to 45 kHz [11]. In addition, energetic electrons driven modes are expected with a frequency above ten kilohertz following the commissioning of ECRH system in the middle of 2019. The high frequency response (phase shift and normalized amplitude) of the Mirnov probes has not yet been investigated and hence is ignored in the MHD mode analysis on J-TEXT. The phase shift can influence the real-time measurement

^a Authors to whom any correspondence should be addressed. E-mail: wangnc@hust.edu.cn

accuracy of the tearing mode location, which is essential for the feedback control [12, 13]. The weak MHD modes will be more difficult to measure due to the strong screening of the high frequency magnetic perturbations.

Therefore, this paper studies the high frequency response of the Mirnov probe on the J-TEXT tokamak, especially on the eddy current effect. A test platform was established to generate uniform AC magnetic field by solenoid within the range of 1-300 kHz. To understand the eddy current effect, the AC magnetic fields with various frequencies are measured by the magnetic probe with two different materials besides, i.e. graphite and 304-stainless steel, located at various distances. It is found that the impact on the eddy currents of the phase and amplitude of the measured magnetic field is non-monotonic with respect to frequency. The eddy current effect is larger if the conducting plate's resistivity is smaller or it is closer to the probe.

This paper is organized as follows. The set-up of the platform and the quantitative definition of the eddy current effect are introduced in Section II. Section III describes a data processing method to cancel the impact of the resonant effect of the Mirnov probe circuit on the measurement. Section IV describes the measurement of the high frequency response of the Mirnov probe under various conditions. Section V introduces the phasor expression of the AC magnetic field and analyzes the eddy current field. Section VI summarizes the paper.

II. EXPERIMENTAL SET-UP

The upgraded Mirnov probe array contains one poloidal array with 48 probe modules and two toroidal arrays with 25 probe modules on J-TEXT tokamak. Mirnov probe is more and more used to measure high frequency MHD instabilities on J-TEXT tokamak. Due to the installation method, there are two kinds of conductor materials [14], 304-stainless steel and graphite, nearby the Mirnov probe, which will cause error in the measurement of magnetic field when the frequency increases. By studying the eddy current effects of these two conductors at different frequencies, the measurement of high frequency magnetohydrodynamic (MHD) instabilities in J-TEXT tokamak can be more accurate.

Therefore, a test platform, which is capable of generating a uniform AC magnetic field, is essential for studying the high frequency response of the Mirnov probe, especially with a conductor nearby. Helmholtz coils are widely used for calibrating and measuring the lumped-circuit parameters of a magnetic inductive probe [5]. However, a very large Helmholtz coil is needed to create a uniform magnetic field region, which is large enough for both the Mirnov probe and the conducting plate. A long straight solenoid is more

suitable for producing such a uniform magnetic field in a large region. Figure 1(a) and (d) displays the schematic diagram of the test platform, which consists of a solenoid, a chute board, a Mirnov probe and a conducting plate made of 304-stainless steel or graphite.

The solenoid has a length of 80 cm and a radius of 10 cm. A copper wire with a diameter of 0.2 cm (12 AWG gauge wire) is wound for 400 turns to form the solenoid, as show in Figure 1(b). A signal generator operating in the frequency range from 1 kHz to 300 kHz is used as the power supply for the solenoid. The finite element simulation shows that the magnetic field within the solenoid is highly uniform, i.e. the axial magnetic field b_0 remains 99.5% of its maximal value in a cylindrical region, centered in the middle of the solenoid with a diameter of 15 cm and a length of 50 cm.

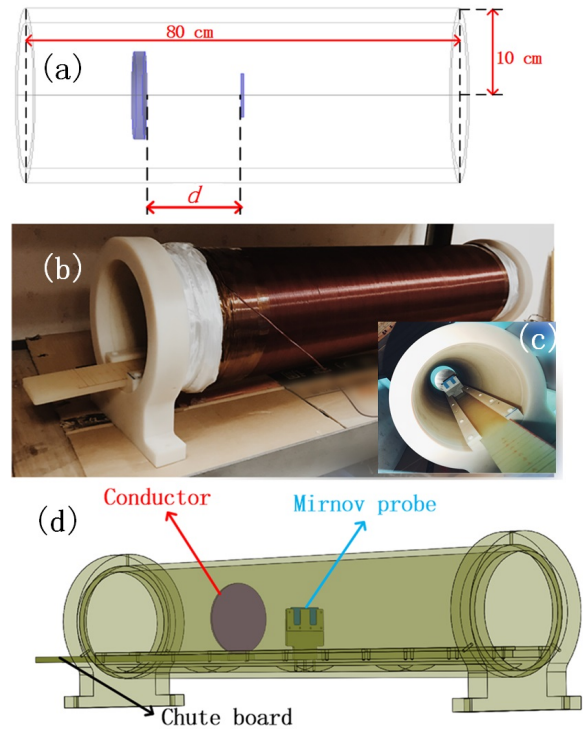


FIG.1 The schematic (a) and design (d) diagram of the test platform, showing the locations of the probe and the conducting plate with d the distance between them. The photograph of the solenoid (b) and the probe and the conducting plate (c).

The Mirnov probe, supported by a W-shaped bracket, is placed with its center located at the center of the solenoid and its axial direction along the axial direction shown in Figure 1(a), hence it measures b_0 . The Mirnov probe is made of a low temperature co-fired ceramic (LTCC), and it is a complicated printed circuit on the ceramic piece with multi layers. It has a thickness of 0.09 cm with a length of 6 cm, width of 3.2 cm and 80 turns. The effective area, NS , of the probe is 884.8 cm² calibrated by Helmholtz coils [14].

The impedance analyzer measures the parameters of the sensor together with the leading wire. It is shown that the inductance, capacitance and the resistance of the sensor is 0.4177 mH, 104.9 pF and 59.8 Ω , which corresponds to a resonant frequency of 759.8 kHz. These parameters indicate a cutoff frequency of 283 kHz with 3 dB attenuation. A circular conducting plate, with a diameter of 12 cm and a thickness of 0.5 cm, is placed parallel to the Mirnov probe with its axis coinciding with that of the solenoid, as shown in Figure 1(a). Figure 1(c) shows the picture of the arrangement of the probe and conducting plate within the solenoid. The conducting plate is installed on a chute board, which can be slid along the axis of the solenoid. This varies the distance between the probe and the conductor, d , from 0.5 cm to 10 cm. Hence, both the conducting plate and the probe are inside the uniform magnetic field region.

In the experiments, the voltage and current of the solenoid and the output voltage of the Mirnov probe were acquired by an oscilloscope. The frequency of the magnetic field is scanned from 1 to 300 kHz, while the programmed output voltage of the power supply is maintained at a constant amplitude of 5 V. The sampling rate is high enough to ensure more than 10000 points per cycle at 300 kHz.

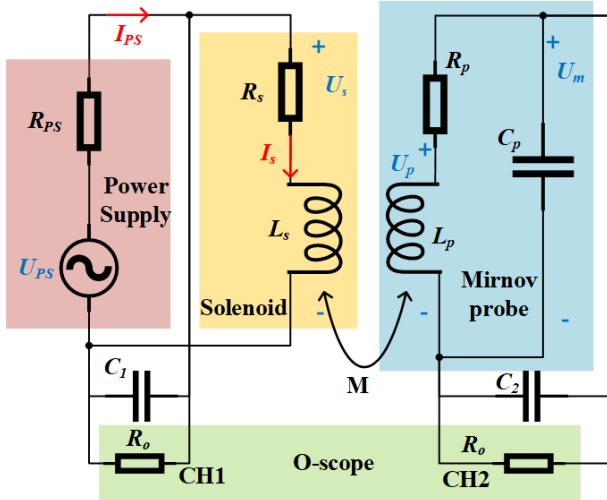


FIG. 2 The driving and measurement circuit of the platform. U_{PS} is the programmed output voltage of the power supply, U_s is the voltage of the solenoid, I_{PS} is the current of the driving circuit, I_s is the current of the solenoid, U_p is the pick-up voltage of the probe; U_m is the measured voltage from the oscilloscope.

Figure 2 displays a model describing both the solenoid and the Mirnov probe-oscilloscope circuits. R_p , R_s , R_{PS} , R_O (CH1 and CH2) are the resistance of the Mirnov probe, the solenoid, the power supply and the oscilloscope; L_p and L_s are the inductance of the Mirnov probe and the solenoid, while M is the mutual inductance between them; C_p , $C_{1(2)}$ are the capacitance of the Mirnov probe and the stray capacitance in the driving (measurement) circuit. Where the RLC parameters of the Mirnov probe is discussed before; R_s

is about 1.3 Ω , R_{PS} is 50 Ω and R_O is 1M Ω ; L_s is about 7mH; C_1 is about 8pF and C_2 is about 170pF. The value of C_1 and C_2 are guessed that make the model qualitatively agree with the data for better analyzing the circuit model. In low frequency range, C_1 , C_2 and R_O can be ignored.

During the test, the input voltage of the solenoid was kept constant and sinusoidal. Hence the input voltage \tilde{U}_{PS} , the current \tilde{I}_s of the solenoid and the equivalent impedance Z_e between \tilde{U}_{PS} and \tilde{I}_s can be described as

$$\tilde{U}_{PS} = U_{PS} \sin(\omega t + \phi_U) \quad (1)$$

$$\tilde{I}_s = I_s \sin(\omega t + \phi_I) \quad (2)$$

$$Z_e = \frac{(R_{PS} + Z_{//})Z_s}{Z_{//}} \quad (3)$$

where ω equals to $2\pi f$, $Z_s = R_s + j\omega L_s$, $Z_{//} = (\frac{1}{Z_s} + \frac{1}{R_O} + j\omega C_1)^{-1}$, I_s and ϕ_I are determined by Z_e as a function of frequency. In this paper, the reference time $t = 0$ is selected with $\phi_U = 0$ by measuring U_{PS} .

According to the Biot-Savart Law, the magnetic field generated by the solenoid should be linear to \tilde{I}_s , i.e.

$$\tilde{B}_0 = k I_s \sin(\omega t + \phi_I). \quad (4)$$

The output voltage of the Mirnov probe, \tilde{U}_p , reflects the time derivative of the magnetic flux, and can be described as

$$\tilde{U}_p = -NS \frac{d\tilde{B}}{dt} = U_p \sin(\omega t + \phi_p) \quad (5)$$

The probe-measured magnetic field \tilde{B} can be obtained by integrating \tilde{U}_p . \tilde{B} is the magnetic field component normal to the surface of the magnetic probe, and \tilde{B} equals to \tilde{B}_0 in the case without conducting plate.

The voltage, current and impedance can be expressed by phasor (phase vector) through frequency domain analysis. The phasor expression allows an easier analysis on the amplitudes and phases of several sinusoidal waveforms, i.e. $\dot{U}_p = U_p e^{j\phi_p}$. In this paper, overdots are used to express phasor (phase vector), the time derivatives are expressed by $\frac{d}{dt}$.

In the measurement circuit, it is found that the relationship between the oscilloscope measured voltage \dot{U}_m and the pick-up voltage of Mirnov probe is \dot{U}_p

$$\dot{U}_p = \frac{Z_r}{R_p + j\omega L_p + Z_r} \dot{U}_m \quad (6)$$

where $Z_r = (j\omega C_p + \frac{1}{R_O} + j\omega C_2)^{-1}$. Defining Z_m as the impedance of the measuring circuit, i.e. $Z_m =$

$$\frac{Z_r}{R_p + j\omega L_p + Z_r}, \text{ the amplitude of } \dot{U}_p, U_p \text{ is}$$

$$U_p = |Z_m| \cdot U_m \quad (7)$$

and the phase of \dot{U}_p, ϕ_p is

$$\phi_p = \phi_z + \phi_m \quad (8)$$

where ϕ_z is the Impedance angle of Z_m , ϕ_m is the phase of \dot{U}_m .

In the low frequency range (e.g. <10 kHz), the impact of the oscilloscope and capacitance C_p in the solenoid and probe circuit were negligible, and hence the oscilloscope measured voltage by the \tilde{U}_m equals to \tilde{U}_p . The relationship between \tilde{U}_m and \tilde{U}_p in the higher frequency range will be discussed in Section III.

Figure 3 shows the waveforms of (a) the current in the solenoid, (b) the output voltages of the Mirnov probe without and with a conducting plate (304 steel) and (c) the measured magnetic field obtained by integrating \tilde{U}_p for cases without and with a conducting plate (304 steel). The signals shown in Figure 3 (a) and (b) were directly acquired by the oscilloscope. A very good signal to noise ratio is clearly observed for \tilde{U}_p . It is found that the phase of the measured magnetic field without any conductor is the same as that of \tilde{I}_s , as described previously in Equation (4). When the 304-stainless steel plate is placed at $d = 1$ cm in the 3.981 kHz AC magnetic field, the amplitude and phase of the probe-measured magnetic field change significantly with respect to the case without any conductor.

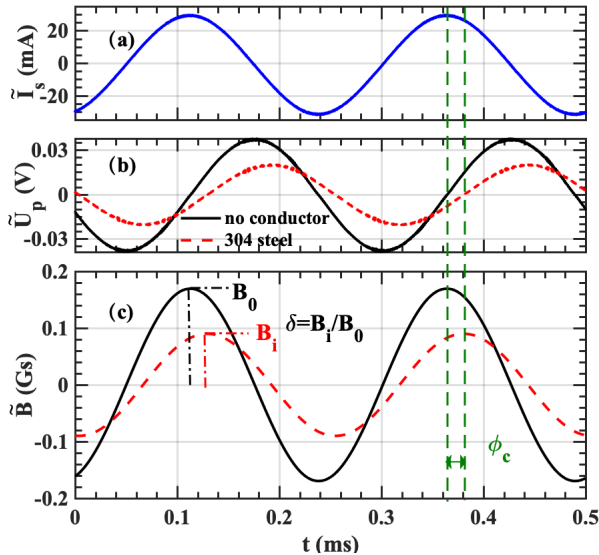


FIG. 3 The raw signal of (a) the current in the solenoid, (b) the probe output voltages in 2 cases without conductor (black) and with stainless steel when $d = 1$ cm (red) at 3.981 kHz. (c) The measured magnetic fields are obtained by integrating \tilde{U}_p for cases without conductor (black) and with stainless steel. The definitions of the normalized amplitude δ and the phase shift ϕ_c due to the eddy current effect are indicated in (c).

The eddy current effect is quantitatively reflected by defining the normalized amplitude δ and phase shift ϕ_c of the measured magnetic field between cases with

and without a conducting plate located near the Mirnov probe, as follows:

$$\delta = \frac{B_i}{B_0} \quad (9)$$

$$\phi_c = \phi_i - \phi_0 \quad (10)$$

where B_i and B_0 (ϕ_i and ϕ_0) are the amplitudes (phases) of the magnetic field with and without a conducting plate, respectively. In this work, the subscripts i and 0 are used to represent the cases with and without conductors, respectively. As defined in Equation (4), $B_0 = kI_s$ and $\phi_0 = \phi_1$. δ and ϕ_c are also marked in Figure 3(c).

III. IMPACT OF THE RESONANT EFFECT OF THE MIRNOV PROBE CIRCUIT ON THE MEASUREMENT

A. MAGNETIC FIELD WITHOUT CONDUCTORS

In this work, both \tilde{B} and \tilde{U}_p are sinusoids with a single frequency. Hence by integrating Equation (5) on both side, \tilde{B} is expressed as $\tilde{B} = \frac{U_p}{2\pi f N S} \sin(\omega t + \phi_p + \pi/2)$. The amplitude and phase of the magnetic field \tilde{B} (B and ϕ) are described as

$$B = \frac{U_p}{2\pi f N S} \quad (11)$$

$$\phi = \phi_p + \frac{\pi}{2}. \quad (12)$$

The nonlinear least square fitting was used to obtain the amplitude and phase of the Mirnov probe output voltage. According to Equation (5), \tilde{U}_p is a sine function of t , hence the fitting function is described as

$$\tilde{U}_p = a_1 \sin(2\pi a_2 t + a_3) + a_4 \quad (13)$$

where a_1 is the amplitude, a_2 is the frequency, t is the time, a_3 is the phase and a_4 is the offset of the signal, with a required fit confidence of 95%. The magnetic field is then obtained by applying Equation (11) and (12).

Figure 4 displays the dependences of the measured magnetic fields and the measured output voltages of probe on frequency in the case without conductors. As shown in Equation (3), the inductive component of Z_e in the solenoid circuit increases with frequency in the frequency range studied here, i.e. 1 kHz to 300 kHz. This leads to the decrease of solenoid current I_s and the increase of phase shift $|\phi_1|$, with a constant solenoid input voltage. Hence, the solenoid magnetic field decreases with the increase of frequency and the phase changes towards -90 degree, as shown in Figure 4(a). The measured voltage U_m increases with

frequency from about 0.025 V to 0.07 V. This indicates that the good signal to noise ratio of \tilde{U}_m holds from 1 to 300 kHz in this work. However, when f is larger than 100 kHz, ϕ_{Bm0} decreases below -90° , ϕ_{m0} decreases below -180° , while U_{m0} shows a significantly increase.

This observation is related to the resonant effect in the measurement circuit, i.e. the frequency dependence of Z_m , with Z_r . Taking into the stray capacitance C_2 and resistance R_o into account, the resonant and cutoff frequency of the Mirnov probe will decrease from 759.8 and 283 kHz towards lower frequency. Hence U_m and B_m increases significantly above 100 kHz, and lead to the decrease of ϕ_{m0} and ϕ_{Bm0} below -180° and -90° respectively.

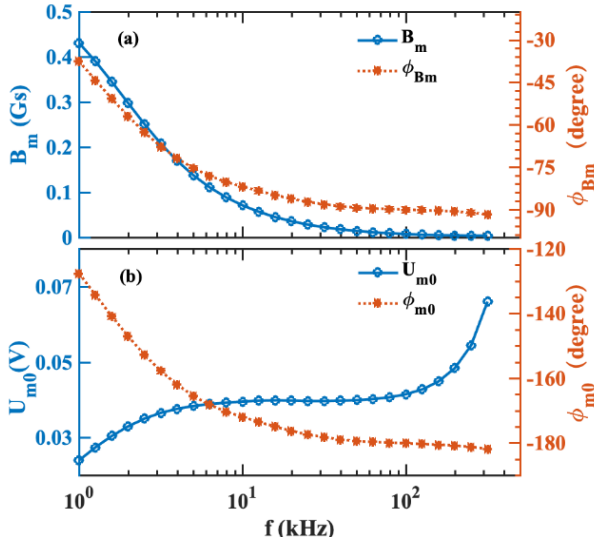


FIG.4 The amplitude and phases of (a) the apparent magnetic field and (b) the apparent output voltage measured by the oscilloscope without the conducting plate.

B. THE METHOD TO CANCEL THE RESONANT EFFECT IN THE EDDY CURRENT STUDY

The results displayed in Figure 4 raise two issues which need to be solved in order to measure δ and ϕ_c . (1) Are the solenoid currents I_s , and hence the solenoid field B_0 , the same between two cases without and with the conducting plate? (2) How will the resonant effect in the Mirnov probe circuit influence the relationship between U_m and U_p (and hence between the measured magnetic field B_m and the actual magnetic field B_p)?

For the first issue, it will be discussed in Section IV that the impact of a conducting plate on the solenoid inductance L_s and resistance R_s is negligible. So I_s and B_0 remain the same after including a conducting plate.

Concerning the second issue, the impact mainly originates from the frequency dependency of Z_m , according to Equation (6). The conducting plate mainly influences L_p via the mutual inductance (M_{cp}) between the conducting plate and the Mirnov probe. It might

reduce L_p slightly and hence modify the resonant frequency of Z_m . According to the model described in Ref. [15], the conducting plate and the probe can be equivalent to two coils with a distance of d , then M_{cp} is calculated. The calculation results show that L_p decreases less than 0.09% with respect to the case without a conducting plate for those f and d studied in this work.

Therefore, the frequency dependency, $Z_m(f)$, is almost the same between the cases without and with a conducting plate, i.e.

$$Z_{mi} = Z_{m0}. \quad (14)$$

Hence $|Z_{mi}| = |Z_{m0}|$ and $\phi_{zi} = \phi_{z0}$. The subscripts 'i' and 'o' refer to the cases with and without a conducting plate for the quantities such as, Z_m , U_m , U_p , ϕ_z , ϕ_m and ϕ_p , following the same regulation defined for Equations (9) and (10).

According to Equations (9), (11) and (7), δ can be described as

$$\delta = \frac{B_i}{B_0} = \frac{U_{pi}}{U_{p0}} = \frac{U_{mi}}{U_{m0}} \quad (15)$$

And from Equations (10), (12) and (8), ϕ_c can be described as

$$\phi_c = \phi_i - \phi_0 = \phi_{pi} - \phi_{p0} = \phi_{mi} - \phi_{m0} \quad (16)$$

Hence, the two issues raised in the beginning of this sub-section are compensated by taking the ratio between U_{mi} (ϕ_{mi}) and U_{m0} (or ϕ_{m0}). Equation (15) and (16) are used in the following section to calculate the normalized amplitude δ and phase shift ϕ_c for the case with a conducting plate.

IV. MEASUREMENT OF HIGH FREQUENCY MAGNETIC RESPONSE WITH TWO KINDS OF CONDUCTING PLATES

In the 304-stainless steel case, the magnetic fields were measured by the Mirnov probe, placed at a distance d of 8cm, 5cm, 3cm, 2cm and 1cm from the 304-stainless steel plate. Figure 5 displays the dependence of δ and ϕ_c on the frequency f of the magnetic field. As f increases, δ and ϕ_c show the different trends. At a specified distance, e.g. $d = 2$ cm, the magnitude of δ dropped rapidly until 10 kHz, where δ reached a constant value of about 0.58. However, the magnitude of δ increased dramatically again with f larger than 100 kHz. The magnitude of ϕ_c increased until 2.5 kHz, but decreased directly without a saturation from this minimal value. At higher f , the magnitude of ϕ_c approached to 0. The dependences of δ and ϕ_c on f are similar for those cases with different d . With d increasing from 1 to 8 cm, the magnitude of δ increased while the magnitude of ϕ_c decreased. This indicates that the eddy current effect reduces with increasing d .

Therefore, when the higher frequency magnetic fluctuations are measured on the J-TEXT tokamak, the phase shift of the eddy current effect with the 304-stainless steel is small. There are two methods to improve the accuracy of the Mirnov probes. One of the methods is using these data of the eddy current effect to compensate experiment data and then obtain the real fluctuation amplitude and phase. The other is to understand the principle of the eddy currents and then changing the material or d so as to reduce the influence of the eddy current on the magnetic measurement.

The amplitude of the eddy currents is influenced by the resistivity of the conductor, specifically reducing the effect with increasing resistivity. Graphite is a higher resistivity material, used as a protective covering for the Mirnov probes. Figure 6 displays the dependences of δ and ϕ_c on f for graphite. At the distance d of 2 cm, the magnitude of δ began to drop at about 10 kHz, then decreased rapidly until 125 kHz. Without a saturation, the magnitude of δ increased again with f larger than 125 kHz. The magnitude of ϕ_c increased slowly until 40 kHz, and decreased towards 0. At different d , the magnitude of δ and the magnitude of ϕ_c also have the similar trend. The normalized amplitude and phase shift were smaller at larger d . At $d = 1$ cm and 250 kHz in Figure 6, δ and ϕ_c diverged from a smooth trend. This has not been understood yet. In conclusion, the eddy current effect with graphite appeared at higher frequency, meaning that graphite permits a more accurate measurement of low-frequency MHD.

It is noted that the impact of the conducting plate on the performance of the solenoid is negligible. The solenoid magnetic field induces eddy currents in the conducting plate; hence, Z_s should be slightly smaller and Z_e should be slightly larger in the case with conductor than the case without conductor. The increase of Z_e with a constant U_{PS} then leads to the reduction of I_s and hence B_0 . It is shown Figure 5 and Figure 6 that $\delta > 0.94$ at $d = 8$ cm for both 304 steel and graphite. The reduction of B_0 due to the increase of Z_e is less than 6%, because there still exists eddy current field at $d = 8$ cm. This is much smaller than the eddy current effect, which can be clearly observed with smaller distance, e.g. 1 cm. However, this slight rise of Z_e is less than 3% according to the modelling by using ANSYS, therefore, the impact of the conducting plate on I_s and B_0 is negligible and the increase on the magnitude of δ is not because of the existence of conducting plate. The eddy current field will be studied quantitatively in Section V.

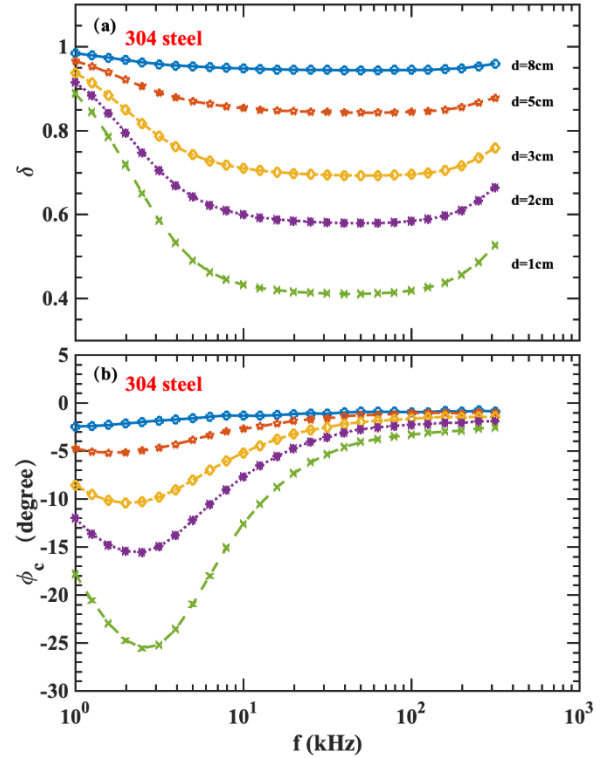


FIG. 5 The dependences of (a) δ and (b) ϕ_c on the frequency of the magnetic field with the 304-stainless steel plate placed at 5 different distances.

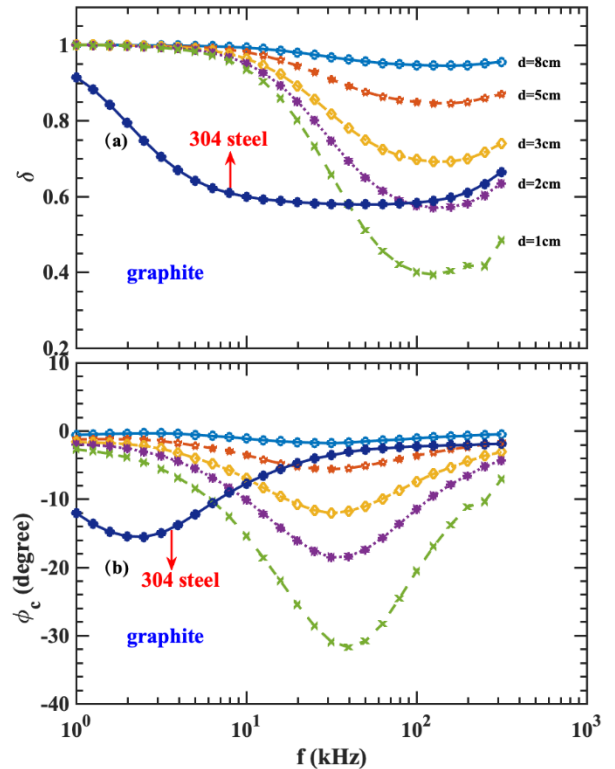


FIG. 6 The dependence of (a) δ and (b) ϕ_c on the frequency of the magnetic field, f , with the graphite plate placed at 5 different distances. The traces for 304 stainless steel at $d = 2$ cm are included for comparison.

V. ANALYSIS OF THE EDDY CURRENT FIELD VIA PHASOR EXPRESSION

The significant increase on the magnitude of δ with f increasing from 100 to 300 kHz indicates that the eddy current effect reduces with f . The decrease of eddy current effect might be related to the change of the skin depth λ with f , which can be described as,

$$\lambda = \frac{1}{\sqrt{\pi f \gamma \mu}} \quad (17)$$

where γ is the conductivity, μ is the magnetic permeability of the conductor and f is the frequency.

To study the eddy current field directly, the phasor can also be used to describe the sinusoidal waveforms of the magnetic fields. The AC magnetic field in Equation (4) can be written in the form of $\dot{\vec{B}} = \text{Im}(B e^{j\phi} e^{j\omega t})$, where B and ϕ are the amplitude and phase of the AC magnetic field. Then the phasor of magnetic field, $\dot{\vec{B}}$, is defined by the time invariant component of the complex value, i.e. $\dot{\vec{B}} = B e^{j\phi}$.

The magnetic field measured by the Mirnov probe $\dot{\vec{B}}_i$ is the linear superposition of the background magnetic field $\dot{\vec{B}}_0$ and the eddy current field $\dot{\vec{B}}_e$, i.e.,

$$\dot{\vec{B}}_i = \dot{\vec{B}}_0 + \dot{\vec{B}}_e \quad (18)$$

$\dot{\vec{B}}_e$ is then normalized to $\dot{\vec{B}}_0$, and $\dot{\vec{B}}'_e = \delta_{ec} \cdot e^{j\phi_{ec}}$ is used to represent the normalized phasor of the eddy current field. δ_{ec} and ϕ_{ec} are the normalized amplitude and relative phase (with respect to $\dot{\vec{B}}_0$) of the eddy current field. According to the Equations (15), (16) and (18), $\dot{\vec{B}}'_e$ can be described as,

$$\dot{\vec{B}}'_e = \frac{\dot{\vec{B}}_e}{\dot{\vec{B}}_0} = \delta \cdot e^{j\phi_c} - 1. \quad (19)$$

Then, δ_{ec} and ϕ_{ec} can be calculated from δ and ϕ_c .

Figure 7 displays the frequency dependence of δ_{ec} , ϕ_{ec} and λ at $d = 2$ cm for both 304 steel and graphite. For the graphite plate, the normalized amplitude of the eddy current field, the magnitude of δ_{ec} , increased with f in the frequency range between 1 and 50 kHz, while the phase ϕ_{ec} decreased from -90° towards -150° . The increase on the magnitude of δ_{ec} indicates that the screening effect becomes more significant due to the increase of inductive voltage which drives larger eddy current, while ϕ_{ec} shows that the inductive component grows dominant to the resistive component in the eddy current circuit. From 50 kHz, the magnitude of δ_{ec} increased slowly with f until 100 kHz, where δ_{ec} reached its maximal and began to decrease with the further increase of f . ϕ_{ec} decreased slowly towards -180° with f . Figure 6(a) gives a direct impression of how the amplitude and phase of eddy current field evolve with f . The relationship between $\dot{\vec{B}}'_e$ and $\dot{\vec{B}}_0$ is

also indicated.

The saturation and decay on the magnitude of δ_{ec} with the increase of f might be related to the change of equivalent resistance in the eddy current circuit. Figure 6(d) shows that the skin depth λ decreased to 2.5 mm, the half thickness of the conducting plate, at 100 kHz. With f increasing beyond 100 kHz, the eddy current concentrates towards to surface and the effective thickness of the eddy current path reduces. This eddy current distribution might reduce the geometric coupling between the eddy current and the Mirnov probe. A similar effect of the decay of eddy current coupling has been reported in Ref. [16]. These analyses indicate that the experimental measurement in J-TEXT is affected by eddy currents and hence proper treatments for correcting the amplitude and phase are necessary, especially for high frequency MHD activities such as the Alfvén Eigenmode (AE).

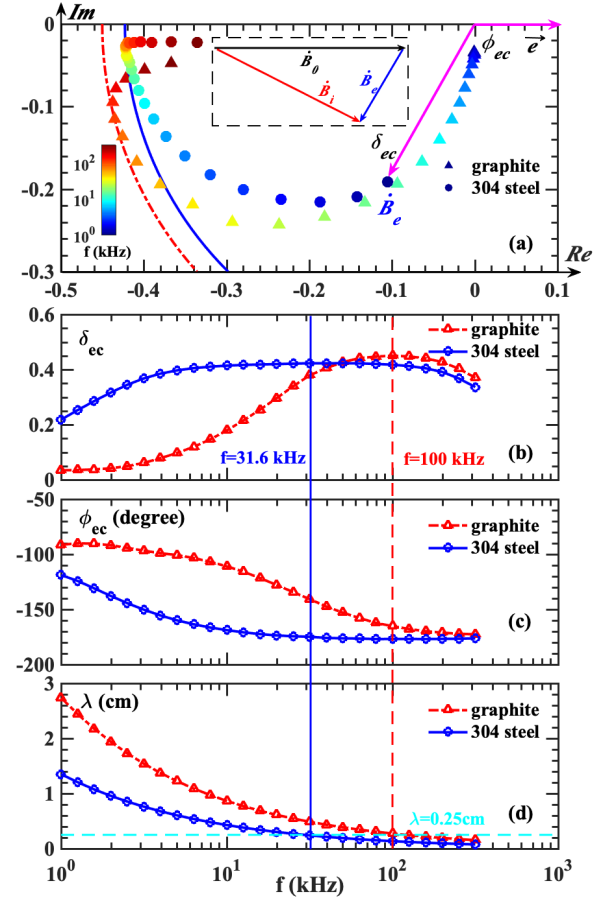


FIG.7 The dependence of (a) phase vector $\dot{\vec{B}}'_e$, (b) δ_{ec} , (c) ϕ_{ec} and (d) λ on f with the graphite and 304-stainless plates placed at 2 cm. The red and blue vertical lines mark the maximal value of δ_{ec} with graphite and 304-stainless steel plates. $\lambda = 2.5$ mm corresponds to the half of the conducting plate thickness.

VI. SUMMARY

This paper investigates the high frequency response of the Mirnov probe based on a test platform, which is capable of generating a uniform AC magnetic

field within the frequency range of 1-300 kHz. The eddy current effect is quantitatively reflected by the phase shift ϕ_c and normalized amplitude δ of the measured magnetic field between cases with and without a conducting plate located near the Mirnov probe. This method compensates the resonant effect in the Mirnov probe circuit, and hence reflects purely the eddy current effect. The eddy current effect increases with the decrease of the distance between the probe and the conducting plate. With the increase of frequency, the magnitude of δ decreases to a saturated value at 10 kHz but increases significantly above 100 kHz for 304-stainless steel, while the eddy current effect with graphite appears at around 10 kHz and the magnitude of δ decreases to the minimum at 125 kHz, followed by a significantly increase above 125 kHz. With the increase of f , the magnitude of ϕ_c increased until 2.5 kHz and 40 kHz for steel and graphite respectively, then decreased with further increase of f .

The phasor expression is introduced to describe the AC magnetic field and allows an easy expression of the eddy current field. The phase of the eddy current field decreases towards -180° with f . The amplitude of the eddy current field increase with f and reaches its maximum when the skin depth reduces to a critical value. The eddy current field decreases with further increase of the frequency.

Last but not least, this experiment did not consider about the size and shape of the conductors, which might influence the eddy current circuit. Besides, it is necessary to verify and quantify the effect of the skin effect on the high frequency response of the Mirnov probe by changing the thickness of the conductor. In addition, reducing the impact of the eddy current effect itself or using more advanced data analysis methods to extract real signals are both methods that can be considered to improve the high frequency response of the Mirnov probe.

ACKNOWLEDGMENTS

The authors are grateful to Dr. B. Rao, Mr. Y. Zhang and Dr. Y. Ma for helpful discussions. This work is supported by the National Magnetic Confinement Fusion Science Program of China (Grant Nos. 2015GB111001) and the National Natural Science Foundation of China (Grant Nos. 11505069).

REFERENCE

- ¹ J. Wesson, *Tokamaks*, 3rd ed. (Clarendon Press, 1987).
- ² H. Hutchinson, *Principles of Plasma Diagnostics* (Cambridge University Press, Cambridge, 1990).
- ³ S. V. Mirnov, I. B. Semenov, *Sov. At. Energy* **30**, 22 (1971).
- ⁴ G. Bateman, *MHD instabilities*, (MIT press, Cambridge, MA 1980).
- ⁵ F. Li, Z. Chen, *et al.*, *Rev. Sci. Instrum* **87**, 066102 (2016).
- ⁶ R. F. Heeter, A. F. Fasoli, *et al.*, *Rev. Sci. Instrum* **71**, 4092

(2000).

- ⁷ M. Schittenhelm, H. Zohm, *et al.*, *Nucl. Fusion* **37**, 1255(1997).
- ⁸ A. Schmid, "Charakterisierung von plasmafluktuationen mit einer kombinierten mirnov-langmuir-sonde am tokamak ASDEX upgrade". Master's Thesis, Technische Universität München, 2005.
- ⁹ L. Horváth, P. Zs. Poloskei, *et al.*, *Plasma Phys. Control. Fusion* **57**, 125005 (2015).
- ¹⁰ Y. Ding, Z. Chen, *et al.*, *Plasma Sci. Technol.* **20**, 125101(2018).
- ¹¹ L. Liu, J. He, *et al.*, *Plasma. Phys. Control. Fusion* **57**,065007 (2015).
- ¹² Q. Hu, Q. Yu, *Nucl. Fusion* **56**, 034001 (2016).
- ¹³ D. Li, Y. Ding *et al.*, *27th IAEA Fusion Energy Conference* (Nov. 22nd - 27th, 2018, Gandhinagar, India), EX/P3-13.
- ¹⁴ D. Guo, Q. Hu, *et al.*, *Rev. Sci. Instrum.* **88**,123502 (2017).
- ¹⁵ Clayton R. Paul, *Inductance: Loop and Partial*, ISBN: 978-0-470-46188-4
- ¹⁶ S. Jiao, X. Liu, *et al.*, *IEEE Trans. Magn.*, **53**, 6201608(2017).